Planar Array of Electrical Capacitance Tomography with Rotation

Maomao Zhang, *Member, IEEE*, Yijun Liu, Manuchehr Soleimani

***Abstract*—This paper investigates a rotational data collection strategy for planar array electrical capacitance tomography (ECT) to improve the imaging of complex-shaped objects in scenarios where access to the object is limited. Planar array of ECT can produce 2D and 3D images of changes in the dielectric permittivity of the object, but detecting complex-shaped objects may require more electrodes in the array, which can decrease the quality of capacitance measurements and make it challenging to detect objects at greater depths. With the air background as calibration measurements, by rotating the sensor array or the object, more independent data can be obtained, which can enhance image quality compared to traditional planar array ECT. The paper presents experimental results of image enhancement through visual reconstruction of known-shaped dielectric test samples and quantitative analysis against the ground truth. These findings suggest that rotational data collection has the potential to improve image quality in planar array ECT for detecting complex-shaped objects.**

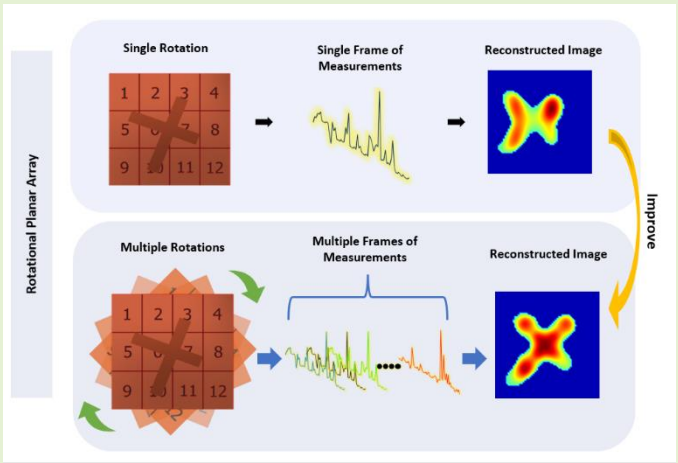

***Index Terms*—Electrical capacitance tomography, planar array imaging, rotational measurement.**

I. Introduction

ELECTRICAL capacitance tomography (ECT) is an imaging system developed for industrial process applications[1-4]. The ECT found new interests in areas such as landmine detection, and soft robotic sensing [5-7]. Planar array of ECT normally includes an array of electrodes on a flat surface capable of imaging in near-surface imaging. ECT is already a well-developed tomography modality. Tomography is a method that is used to detect the inner construction of material under test (MUT) by capacitance, which is a non-destructive method. This experiment detects the dielectric distribution in the material. When the material distribution (dielectric distribution) in the object changes the permittivity varies because different dielectric has different permittivity. The principle of ECT is measuring the capacitance between electrode pairs and constructing the dielectric permittivity distribution image. Not only typical Tikhonov-based reconstruction [8] but also more advanced total variation-based algorithms are used for ECT image reconstruction [5].

Rotational measurement was introduced in [9, 10] for circular sensor array of ECT and has since shown a big improvement in imaging quality. Planar ECT is an emerging area of this tomographic imaging technique, which has found applications in industrial process tomography and material inspection. The main reasons for adopting rotational ECT in the circular array were to produce more independent measured data aiming to enhance the image resolution and quality while maintaining larger area ECT electrodes which is essential for a high signal-to-noise ratio. The same reasons will stand in planar array ECT. In this paper, a rotational planar ECT (RPECT) system has been developed, in which an electrode array can be rotated concerning a central axis perpendicular to the plane of the planar array. The RPECT can produce images with better quality because of increasing the number of independent measurements. A 12-electrode ECT sensor system has been developed to generate the experimental data required in this study. To show the proof-of-principle, a rotational scheme has been implemented with 16 and then 36 steps around 360 degrees. The advantages of the RPECT system have been established using experimental evaluation.

The RPECT can be used in assessing the subsurface condition of carbon fiber-reinforced polymer (CFRP) composite structures [11, 12], since it will provide images of better quality, and the seal integrity inspection for good quality packaging [13]. For robotic touch sensing using planar array of ECT [2, 11] a rotational sensor can be able to identify the more accurate shape of an object. All these applications with RPECT will come with the caveat of longer data collection time, which may be feasible for some applications. This paper focuses on demonstrating the image enhancement within the plane rotation. The concept presented here can be further expanded to the translation movement of the object along the sensor and rotation and rotation with tilting.

Maomao Zhang and Yijun Liu are with the Tsinghua Shenzhen International Graduate School, Shenzhen 518055, China. (e-mail: zhangmaomao@sz.tsinghua.edu.cn, liuyj22@mails.tsinghua.edu.cn).

Manuchehr Soleimani is with the Department of Electronic and Electrical Engineering, University of Bath, Bath BA2 7AY, U.K. (e-mail: M.Soleimani@bath.ac.uk).

II. ECT System

A complete planar array ECT system encompasses three distinct tasks: sensing the object, acquiring data, and image reconstruction. These tasks are further divided into three sub-systems: an array capacitance sensor, a data acquisition and processing hardware, and an image reconstruction software and display, as shown in Fig. 1. The ECT sensor, measuring 200 mm by 200 mm, features a 3 × 4 electrode array, which provides a high signal-to-noise ratio (SNR) level and detection depth while maintaining superior imaging performance. The ECT measurement system employed in this study operates at a frequency of 1.25 MHz, enabling a low-frequency approximation to Maxwell's equation.

The electrical potential can be described as

$$\nabla \cdot (\varepsilon \nabla u) = 0 \qquad (1)$$

where ε is permittivity and u is the electric potential. The capacitance for a given voltage difference V can be divided by the electric charge with a surface integral of electric flux through an area, the capacitance can be defined as

$$C = \frac{1}{V} \oint_{\Omega} \varepsilon \nabla u \, dS \qquad (2)$$

where V is the excitation voltage, Ω is the surface area made up of elements dS.

In ECT forward model, the capacitance is a function of dielectric permittivity given the geometry of electrodes and the voltage used. The forward model can be solved using the finite element method [7] or the finite difference method [5]. For n electrodes, there are n(n-1)/2 independent capacitance measurements that can be used in ECT.

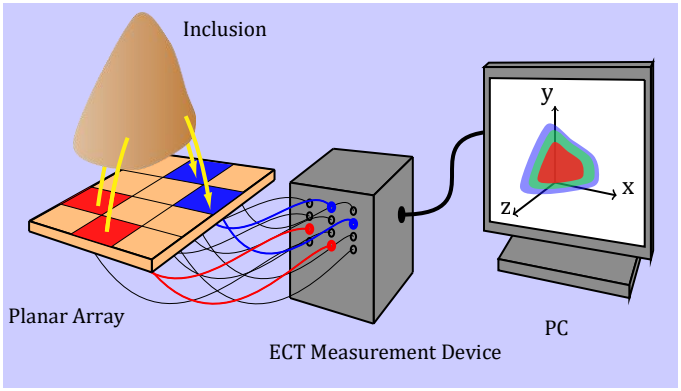

Fig. 1. ECT sensor system for planar array ECT

Fig. 2 shows the simulated data and experimental data for free space measurements for a 12 electrodes planar array electrode ECT sensor, which is 66 measurements.

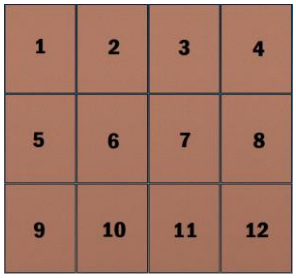

(a)

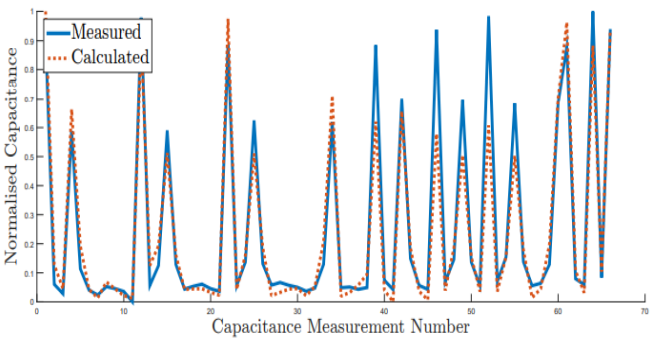

(b)

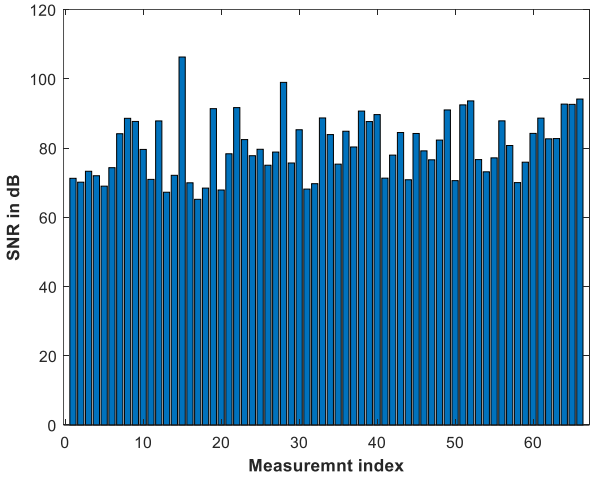

(c)

Fig. 2. (a) Sensor array (b) simulated and experimental data (c) SNR values for all 66 measurements

In addition to the dynamic range of the measurements as it is shown in Fig. 2 the SNR provides a good indication of the imaging sensor performance. The SNR can be described as:

$$SNR_{dB} = \frac{1}{M}\sum_{i=1}^{M} 10\log\left(\frac{\frac{1}{K}\sum_{j=1}^{K}(C_{i,j})}{\sqrt{\frac{1}{K}\sum_{j=1}^{K}\left((C_{i,j}-\overline{C_i})^2\right)}}\right) \qquad (3)$$

where K=66 measurements are repeated N times, we choose M=100 to have a large enough sample size to get a good estimate of the SNR. **Fig**. 2(c) shows the SNR plot for a 12-channel array, with average SNR of 80 dB.

In general, the relationship between measured capacitance and permittivity of the domain is nonlinear. When a small perturbation happens in permittivity $\Delta\varepsilon$, a change in capacitance measurements, ΔC, can be obtained. The relationship between them can be then established by linearizing equation (2) through Taylor expansion

$$\Delta C = S\Delta\varepsilon \qquad (4)$$

where $\boldsymbol{S}$ is the so-called sensitivity matrix or called the Jacobian matrix. To bridge the changes in permittivity distribution and the changes in capacitance measurements, a sensitivity matrix $\boldsymbol{S}$ is built in the following equation (5)**,** by integrating the gradient of electrical potential over the volume of image voxel where electrode i acts as a transmitter and when electrode j acts as a transmitter, for given $\boldsymbol{V_0}$ excitation voltage.

$$S = \frac{\partial C_{ij}}{\partial \varepsilon(x,y,z)} = -\frac{1}{V_0}\int_{\Omega} \nabla u^i(x,y,z) \cdot \nabla u^j(x,y,z) dv \quad (5)$$

III. Combined Image Reconstruction

This paper explores the potential benefits of rotating the sensor array or object under test to generate a greater amount of high-quality measured data. Fig. 3 displays the singular value decay of the RPECT system, ranging from one angle to 16 rotations [14], which provides ample independent data to demonstrate the improvements in image resolution and quality while highlighting the trend of singular values approaching saturation in the image. The figure indicates that the number of singular values increases, suggesting that combining rotational data can yield additional information. However, the total number of singular values above a certain noise level may become saturated as the number of rotation steps increases. Therefore, while a rotational system can provide extra information, its potential gains are ultimately limited by the original sensor structure, particularly the total number of electrodes and the SNR level of the measurement device. The use of a large number of electrodes in a planar array can lead to smaller electrode sizes, resulting in lower quality measured data in terms of SNR and potentially limiting the detection depth of the planar array. However, for cases in which the planar array does not detect an object in depth, rotational ECT can produce a high-quality image, akin to the Radon Transform used in X-ray CT. The present study focuses on large-area electrodes, as the smaller number of electrodes in a planar array has proven effective for depth detection and 3D near subsurface imaging[5].

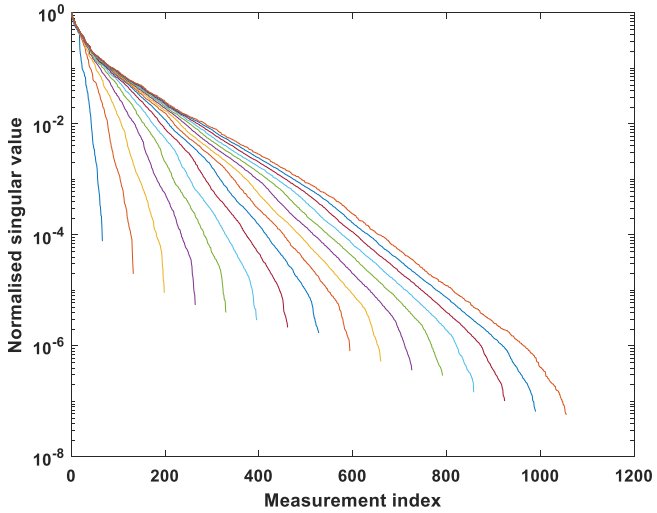

Fig. 3. Singular value decay plot showing increasing numbers of rotations

The inverse problem of generating a permittivity distribution using Jacobian and capacitance measurements data is typically an ill-posed problem, necessitating a regularization scheme for stabilized solutions. One simple method for this task is Linear Back Projection (LBP), which can be enhanced by incorporating regularisation terms, such as Tikhonov Regularization[8]. A more advanced method for planar array ECT sensors is based on total variation (TV) regularization, which enables better depth detection [5]. The ill-posedness and information content of the Jacobian matrix lie at the heart of the inverse problem. Planar array ECT encounters various challenges associated with the ECT inverse problem, including nonlinearity, ill-posedness, and non-uniformity. Increasing the number of electrodes can yield additional measurements and therefore enhance image quality. However, when the number of electrodes increases for a given sensor area, the area allocated to each electrode decreases. According to (2), this reduction leads to smaller capacitance values, making measurements more susceptible to noise.

For image reconstruction, a linear imaging algorithm based on the TV method is used. The Jacobian matrix is calculated for free space in 20 × 20 × 20 voxels for 3D imaging and in 64 × 64 pixels when reconstructing a 2D image. With no rotation, we have 66 measured data, for one rotation we have 66 × 2, data, and finally for 15 rotations (16 angles). The total number of measurement data is 66 × 16. In each case, all measured data are used to do a simultaneous reconstruction using all data. The free space Jacobian matrix is also adapted according to each rotation so that the appropriate Jacobian matrix is used when combining rotational data.

Taking the linear relationship in equation (2) where $\Delta C \in \mathbb{R}^{m1}$, the combined capacitive measurement can be described as $\Delta K \in \mathbb{R}^{m2}$, $\Delta\boldsymbol{\varepsilon} \in \mathbb{R}^{n}$, $S_R \in \mathbb{R}^{m1\times n}$, and $S_M \in \mathbb{R}^{m2\times n}$ and the combined Jacobian matrix $\tilde{S} \in \mathbb{R}^{(m2)\times n}$. $m1$ is 66 measurement for each given angel, and $m2$ is combined data and goes from 66 × 2, 66 × 3..., 66 × 16, n is the number pixels 2D or voxels 3D. To avoid redundant information, the least-square problem can be written as

$$\underset{\Delta\boldsymbol{\varepsilon}}{argmin}\ \varphi(\Delta\boldsymbol{\varepsilon}) \qquad s.t.\ \left\|\tilde{S}\Delta\boldsymbol{\varepsilon} - \Delta K\right\|_2^2 < \delta, \quad (6)$$

where $\varphi(\Delta\boldsymbol{\varepsilon})$ is the convex regularization function which carries the prior information of the unknown permittivity of the test object.

Since the challenge for all soft-field imaging modalities including ECT the combined inverse problem is still ill-posed, the regularization term needs to be added to (6).

As Fig. 3 shows the combination of rotational data is significantly enhancing the ill-posedness of the data, but this still needs regularization.

In this paper, the 3D total variation (TV) regularization method an iterative linear reconstruction is applied with an augmented Jacobian $\tilde{S}$.

$$\begin{aligned} &arg\ \underset{\Delta\boldsymbol{\varepsilon}}{min}\left\|\nabla_{x,y,z}\Delta\boldsymbol{\varepsilon}\right\|_1 \\ &s.t.\left\|\tilde{S}\Delta\boldsymbol{\varepsilon} - \Delta K\right\|_2^2 < \delta \end{aligned} \quad (7)$$

The first term in (7) corresponds to spatial regularization (in x, y, and z directions), and the second term is data fidelity. The analysis of the SNR on the measurement process helps with the data fidelity term in particular deciding when to stop the iterative reconstruction process.

The augmented Jacobian $\tilde{S}$ works on a frame-by-frame basis by combining the Jacobian matrix. To effectively solve the constrained problem, the Bregman iteration is used in this work to convert the constrained problem (7) to an iterative scheme[15].

$$\Delta\boldsymbol{\varepsilon}^{i+1} = arg\ \underset{\Delta\boldsymbol{\varepsilon}}{min}\left\|\nabla_{x,y,z}\Delta\boldsymbol{\varepsilon}\right\|_1 + \frac{1}{2}\left\|\tilde{S}\Delta\boldsymbol{\varepsilon} - \Delta K^i\right\|_2^2 \quad (8a)$$

$$\Delta K^{i+1} = \Delta K^i - \tilde{S}\Delta\boldsymbol{\varepsilon}^{i+1} + \Delta K \quad (8b)$$

As the L1-norm function has the non-differentiability characteristic, the split Bregman method is applied to extend the minimization of the L1-norm regularization terms, where the L1- and L2- functions can be solved in separate steps. With the splitting technique, (8a) can be rewritten as

$$\begin{aligned} \left(\Delta\boldsymbol{\varepsilon}^{i+1}, d_x, d_y, d_z\right) = arg\ &\underset{\Delta\boldsymbol{\varepsilon},d_x,,d_y,d_{yz}}{min}\left\|d_x, d_y, d_z\right\|_1 \\ &+ \frac{1}{2}\left\|\tilde{S}\Delta\boldsymbol{\varepsilon} - \Delta K^i\right\|_2^2 \end{aligned} \quad (9a)$$

$$d_x = \nabla_x \Delta\boldsymbol{\varepsilon}, d_y = \nabla_y \Delta\boldsymbol{\varepsilon}, d_z = \nabla_z \Delta\boldsymbol{\varepsilon}, \quad (9b)$$

where d_x, d_y, d_z are directional derivatives for permittivity changes allowing for anisotropic TV regularisation.

In the case of 2D reconstruction, we use a 2D version of the above iterative TV algorithm.

Root means square error (RMSE) against the true object image, and image cross-correlation (CC) is used to evaluate the enhancement gained by combining rotational data. A lower value of RMSE is desired and a CC value close to 1 indicates at the correct shape is reconstructed[16].

$$RMSE = \sqrt{\sum_{n=1}^{N} (\widehat{x_n} - x_n^*)^2} \quad (10)$$

$$CC = \frac{\sum_{n=1}^{N} (\widehat{x_n} - \widehat{x_a})(x_n^* - x_a^*)}{\sqrt{\sum_{n=1}^{N} (\widehat{x_n} - \widehat{x_a})^2 (x_n^* - x_a^*)^2}} \quad (11)$$

where $\widehat{x_n}$ is the gray value of the nth pixel in the reconstructed image $\hat{x}$, x_n^* is the gray value of the nth pixel in the ground truth image x^*, $\widehat{x_a}$ and x_a^* denote the average value of the gray values of them respectively.

IV. Experiments And The Results

This study presents an evaluation of the 2D and 3D image reconstruction methods for a 3D printed object using differential data collected from a sensor array without rotation and with rotation up to 16 angles (i.e., from 0 to 360 degrees in increments of 22.5 degrees). The results and evaluation of the reconstruction are illustrated in Fig. 4, which includes three sets of images labeled as (A), (B), and (C). The first image in each set displays the 3D structure of different objects, while the second and fourth images depict the reconstructed results in 2D and 3D, respectively, under varying rotational angles. The image quality is progressively enhanced as more rotational angles are included in the image reconstruction, as demonstrated in a_3, b_3, and c_3 of Fig. 4, where the root mean square error (RMSE) decreases and the correlation coefficient (CC) increases with the addition of more rotational angles. A planar array 2D surface imaging method similar to that proposed in [17] is employed in this work.

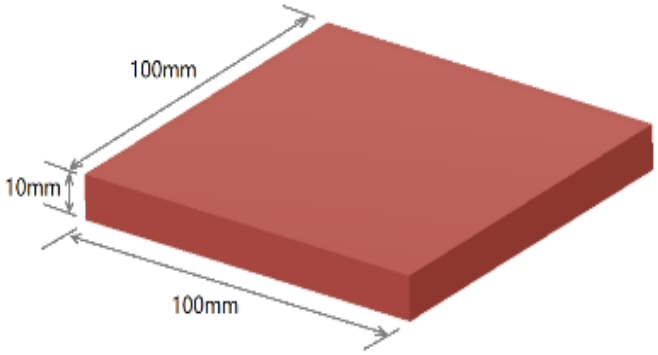

(a_1)

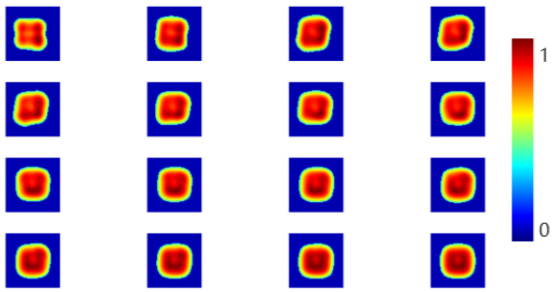

(a_2)

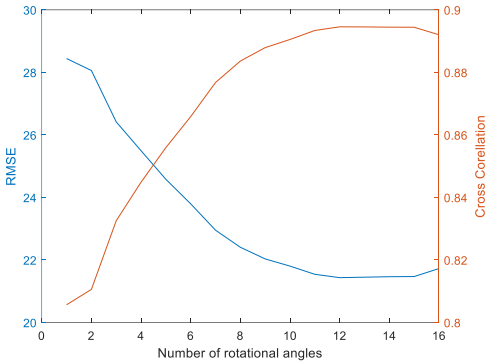

(a_3)

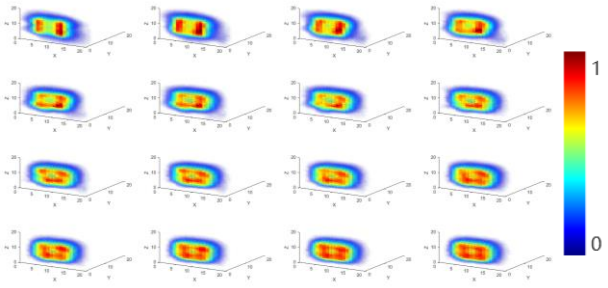

(a_4)

(A)

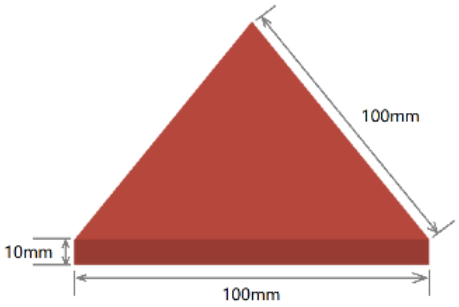

(b_1)

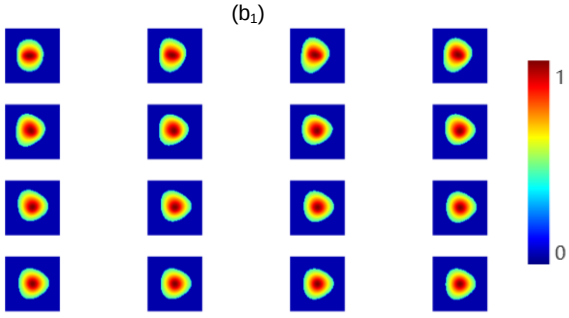

(b_2)

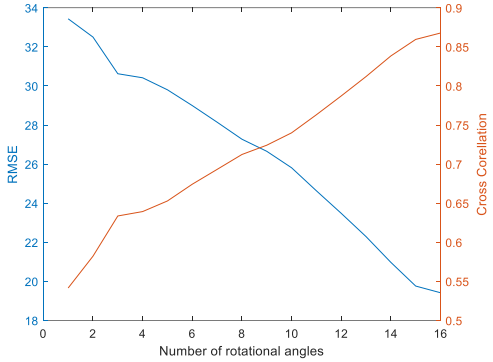

(b_3)

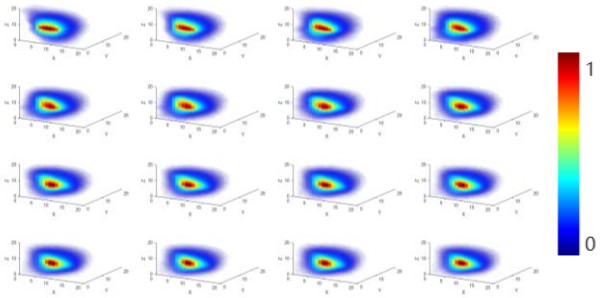

(b_4)

(B)

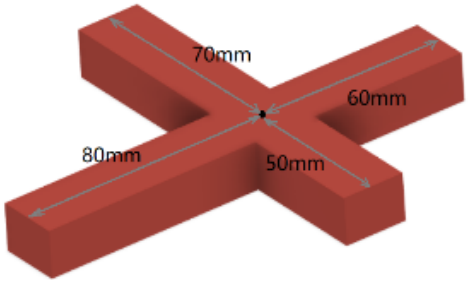

(c_1)

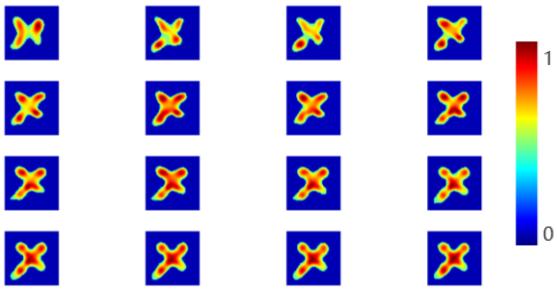

(c_2)

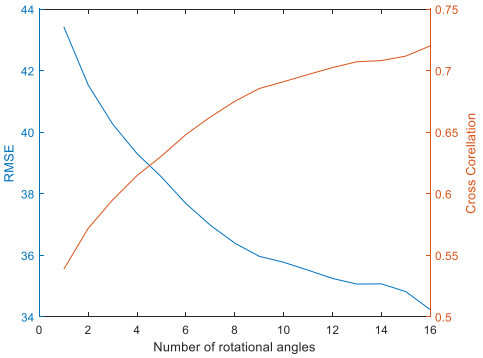

(c_3)

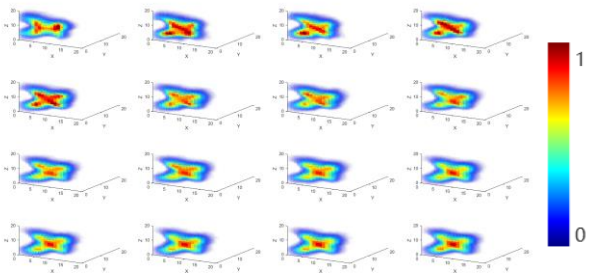

(c_4)

(C)

Fig. 4. Reconstructed images from the square, triangular, and cross-shaped objects, (A) square shape object, (B) triangular shape object, and (C) cross shape object

With rotational angles used in combination, the image quality can be further enhanced [18]. To this end, a set of 36 angles data (every 10 degrees) for triangular shape objects was collected. Fig. 5 shows the RMSE plot (note the value of 16.6 when all 36 angles are used in combination, the value is 19.1 when 16 rotations are used) and CC (0.89 when 36 angles are used, where it was 0.85 when 16 angles of rotation were used). This shows that the refined rotations can lead to a more accurate final image compared to 16 rotations.

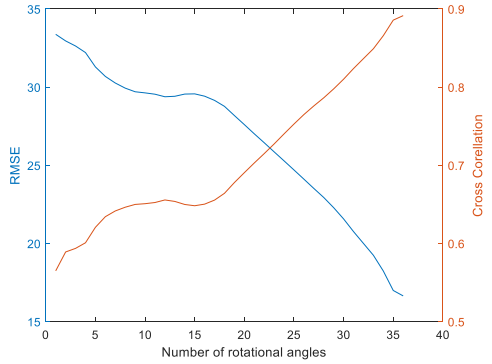

Fig.5. RMSE and CC for triangular shape object when 36 rotational angles are used.

V. Conclusions

This study proposes a planar array ECT system with a rotational feature for imaging dielectric objects. A simple yet effective rotational scheme has been implemented into planar array imaging. The rotational ECT described in this paper demonstrates proof of concept of a method that can improve image resolution without requiring a more complicated hardware ECT system.

A fundamental challenge in planar ECT imaging is obtaining high-quality images at a distance or depth. Simply increasing the number of electrodes to achieve this is not a viable solution, as it would decrease the size of each electrode and make measurements more susceptible to noise. The proposed rotational system, however, maintains the size of the sensors while collecting more independent measurement data. By taking finer steps of rotation and gathering more independent measurements, this system could further improve the image quality, as demonstrated by the image quality enhancement obtained when combining 36 rotational angles instead of 16. It is also important to

know that more rotational angles require more data collection time, and a balance must be reached in the real applications of rational ECT.

To determine an appropriate approach for rotation, one must consider the nature of the application. Objects can either be rotated in front of the sensor array or the sensor array can be rotated in front of a test object. It is important to note that rotation is a mechanical task that will take additional time. Hence, it is only suitable for situations where an accurate identification of an object is needed and sufficient time is available for rotation.

It is worth noting that the ECT sensor is sensitive to any external objects, as well as the object under investigation. Therefore, the rotational system must not leave a harmful footprint on the ECT sensor. Nevertheless, the rotational planar array offers an opportunity to identify more complex shaped objects, which could unlock new applications in different fields.

REFERENCES

[1] H. Wang, D. Hu, M. Zhang, N. Li, and Y. Yang, "Multiphase flowrate measurement with multi-modal sensors and temporal convolutional network," *IEEE Sensors Journal*, 2022.

[2] L. Zhu, Y. Jiang, Y. Li, W. Lu, and M. Zhang, "Conductivity prediction and image reconstruction of complex-valued multi-frequency electrical capacitance tomography based on deep neural network," *IEEE Transactions on Instrumentation and Measurement*, vol. 71, pp. 1-10, 2021.

[3] H. Wang and W. Yang, "Application of electrical capacitance tomography in circulating fluidised beds–A review," *Applied Thermal Engineering*, vol. 176, p. 115311, 2020.

[4] H. Zhu, J. Sun, L. Xu, W. Tian, and S. Sun, "Permittivity reconstruction in electrical capacitance tomography based on visual representation of deep neural network," *IEEE Sensors Journal*, vol. 20, no. 9, pp. 4803-4815, 2020.

[5] C. Tholin-Chittenden and M. Soleimani, "Planar array capacitive imaging sensor design optimization," *IEEE Sensors Journal*, vol. 17, no. 24, pp. 8059-8071, 2017.

[6] T. Schlegl, T. Kröger, A. Gaschler, O. Khatib, and H. Zangl, "Virtual whiskers—Highly responsive robot collision avoidance," in *2013 IEEE/RSJ International Conference on Intelligent Robots and Systems*, 2013: IEEE, pp. 5373-5379.

[7] Z. Ye, R. Banasiak, and M. Soleimani, "Planar array 3D electrical capacitance tomography," *Insight-Non-Destructive Testing and Condition Monitoring*, vol. 55, no. 12, pp. 675-680, 2013.

[8] A. Neubauer, "Tikhonov regularisation for non-linear ill-posed problems: optimal convergence rates and finite-dimensional approximation," *Inverse problems*, vol. 5, no. 4, p. 541, 1989.

[9] C.-N. Huang, F.-M. Yu, and H.-Y. Chung, "Rotational electrical impedance tomography," *Measurement Science and Technology*, vol. 18, no. 9, p. 2958, 2007.

[10] Z. Liu, L. Babout, R. Banasiak, and D. Sankowski, "Effectiveness of rotatable sensor to improve image accuracy of ECT system," *Flow Measurement and Instrumentation*, vol. 21, no. 3, pp. 219-227, 2010.

[11] Z. Cui, Y. Sun, L. Zhang, and H. Wang, "Planar Electrical Capacitance Tomography Dynamic Imaging for Non-destructive Test," *IEEE Transactions on Instrumentation and Measurement*, 2022.

[12] S. Gupta, H. E. Kim, H. Kim, and K. J. Loh, "Planar capacitive imaging for composite delamination damage characterization," *Measurement Science and Technology*, vol. 32, no. 2, p. 024010, 2020.

[13] J. Pan *et al.*, "Non-destructive online seal integrity inspection utilizing autoencoder-based electrical capacitance tomography for product packaging assurance," *Food Packaging and Shelf Life*, vol. 33, p. 100919, 2022.

[14] P. C. Hansen, *Rank-deficient and discrete ill-posed problems: numerical aspects of linear inversion*. SIAM, 1998.

[15] G. Ma and M. Soleimani, "A versatile 4D capacitive imaging array: a touchless skin and an obstacle-avoidance sensor for robotic applications," *Scientific Reports*, vol. 10, no. 1, pp. 1-9, 2020.

[16] Z. Wang, A. C. Bovik, H. R. Sheikh, and E. P. Simoncelli, "Image quality assessment: from error visibility to structural similarity," *IEEE transactions on image processing*, vol. 13, no. 4, pp. 600-612, 2004.

[17] X. H. Hu and W. Q. Yang, "Planar capacitive sensors - designs and applications," (in English), *Sensor Review*, vol. 30, no. 1, pp. 24-39, 2010 2010, doi: 10.1108/02602281011010772.

[18] Y. Capdeboscq, H. Mamigonians, A. Sulaimalebbe, and V. Tshitoyan, "Combining Radon transform and electrical capacitance tomography for a 2d+ 1 imaging device," *Inverse Problems*, vol. 34, no. 10, p. 104001, 2018.